Atmospheric Environment 182 (2018) 105–114

Contents lists available at ScienceDirect

Atmospheric Environment

journal homepage: www.elsevier.com/locate/atmosenv

Local and remote black carbon sources in the Metropolitan Area of Buenos Aires

Melisa Diaz Resquin[a,b,c], Daniela Santágata[a,b], Laura Gallardo[c,e], Darío Gómez[a], Cristina Rössler[a,d], Laura Dawidowski[a,d,*]

[a] Comisión Nacional de Energía Atómica, Gerencia Química, Av. Gral. Paz 1499, B1650KNA San Martín, Pcia. Buenos Aires, Argentina
[b] Facultad de Ingeniería, Universidad de Buenos Aires, Av Paseo Colón 850, C1063ACV, Buenos Aires, Argentina
[c] Center for Climate and Resilience Research (CR)^2, Blanco Encalada 2002, Santiago, Chile
[d] Universidad Nacional de San Martín, Instituto de Investigación e Ingeniería Ambiental, 25 de Mayo y Francia, B1650KNA San Martín, Pcia. Buenos Aires, Argentina
[e] Departamento de Geofísica, Universidad de Chile, Blanco Encalada 2002, Santiago, Chile

ARTICLE INFO

Keywords:
Biomass burning
Fossil fuels
Aerosols
Black carbon
Megacity

ABSTRACT

Equivalent black carbon (*EBC*) mass concentrations in the fine inhalable fraction of airborne particles ($PM_{2.5}$) were determined using a 7-wavelength Aethalometer for 17 months, between November 2014 and March 2016, for a suburban location of the Metropolitan Area of Buenos Aires (MABA), Argentina. In addition to describing seasonal and diurnal black carbon (BC) cycles for the first time in this region, the relative contributions of fossil fuel and remote and local biomass burning were determined by distinguishing different carbonaceous components based on their effect on light attenuation for different wavelengths. Trajectory analyses and satellite-based fire products were used to illustrate the impact of long-range transport of particles emitted by non-local sources. EBC data showed a marked diurnal cycle, largely modulated by traffic variations and the height of the boundary layer, and a seasonal cycle with monthly median EBC concentrations (in $\mu g/m^3$) ranging from 1.5 (February) to 3.4 (June). Maximum values were found during winter due to the combination of prevailingly stable atmospheric conditions and the increase of fossil fuel emissions, derived primarily from traffic and biomass burning from the domestic use of wood for heating. The use of charcoal grills was also detected and concentrated during weekends. The average contribution of fossil fuel combustion sources to *EBC* concentrations was 96%, with the remaining 4% corresponding to local and regional biomass burning. During the entire study period, only two events were identified during which *EBC* concentrations attributed to regional biomass burning accounted for over 50% of total *EBC*; these events demonstrate the relevance of agricultural and forestry activities that take place far from the city yet whose emissions can affect the urban atmosphere of the MABA.

1. Introduction

BC aerosols are produced by the incomplete combustion of fossil fuels and biomass (Bond et al., 2013; UNEP, 2011). BC is defined as an optimal light absorbing substance composed of carbon and which presents five essential characteristics (Bond et al., 2013): i) carbonaceous particulate matter with a graphite-like structure containing a large fraction of sp2-bonded carbon atoms, ii) consisting of spherules aggregates of $<10nm$ to approximately 50 nm in diameter in a fractal-like chain, iii) refractory, iv) insoluble in any solvent, and v) strongly light absorbing across the entire visible spectrum, with a mass-specific absorption coefficient typically greater than 5 m^2/g at 550 nm for newly produced particles. Existing methods cannot, however, quantify all five of these properties simultaneously. In the absence of a method for uniquely determining the BC mass, some authors recommend that the term BC be used as a qualitative and descriptive term, while a distinctive terminology referring to the specific measurement method should be used for the purpose of reporting data (Petzold et al., 2013). For this investigation, we have adopted *EBC* terminology for reporting BC, as recommended by Petzold et al. (2013) for measurements derived from optical methods (given that the Aethalometer uses an optical attenuation method to estimate BC concentrations). Optical BC estimates generally show good agreement with elemental carbon measurements using thermal techniques (Jeong et al., 2004).

More than 80% of people living in urban areas that monitor air pollution are exposed to air quality levels that exceed the World Health Organization (WHO) limits. While all regions of the world are affected, populations in low-income cities are the most impacted. Rapid

* Corresponding author. Comisión Nacional de Energía Atómica, Gerencia Química, Av. Gral. Paz 1499, B1650KNA San Martín, Pcia. Buenos Aires, Argentina.
E-mail address: dawidows@cnea.gov.ar (L. Dawidowski).

https://doi.org/10.1016/j.atmosenv.2018.03.018
Received 10 November 2017; Received in revised form 7 March 2018; Accepted 9 March 2018
Available online 14 March 2018

urbanization in Latin America, where more than 80% of the population lives in cities (Zhu et al., 2013), demands a better understanding of these implications. The Metropolitan Area of Buenos Aires (MABA) is Argentina's largest urban agglomeration and, as in many other megalopolis, combustion-related aerosol levels are influenced by local urban activities. Fuels combusted in this area includes: (i) natural gas, the fuel widely burned in this region by stationary sources in households, industry, institutions and power plants; this fuel is also burned in road transportation; (ii) liquid fuels, mostly burned by mobile sources and three large power plants, mostly during winter; (iii) liquifed petroleum gas (LPG), in low income households, and (iv) wood and charcoal, almost exclusively for grilling. Coal is practically not burned in the MABA. Regarding particulate matter, and according to current inventories (D'Angiola et al., 2010; Oreggioni, 2010), traffic emissions are responsible for 72% of the total emissions of inhalable particles, followed by power plants, accounting for 18%.

Open biomass burning throughout South America contributes significantly to global BC levels; this occurs mainly during the Southern Hemispheres spring and is largely related to deforestation, with land clearing often resulting in prescribed savanna burning for agricultural use within the region Pereira et al. (2009). The spatial distribution of these sources is diverse and spans almost the entire continent, with most sources located hundreds or thousands of kilometers away from Buenos Aires. Nevertheless, BC and gases emitted by these fires have the potential to be transported long distances and can reach the flat terrain of the La Plata river basin where Buenos Aires is located and affect the urban atmosphere Pereira et al. (2011). The use of wood and charcoal for residential heating during winter, especially in low income neighborhoods far from the downtown area, and the combustion of firewood and charcoal for barbecue, which takes place predominantly during weekends and holidays, also represent important sources of local emissions.

The aim of this study was to assess BC levels and their temporal variability in a high traffic area of MABA, and to identify the roles of primary local and regional sources of emissions from fossil fuel combustion and biomass burning. For this purpose, a monitoring campaign was carried out from November 2014 to March 2016. Previous studies in this area have investigated the sources of particulate matter in Buenos Aires, with focuses varying from sea salt markers Dos Santos et al. (2012), to metal profiles Fujiwara et al. (2011), and the role of volcanic eruptions Ulke et al. (2016), while other researchers have studied $PM_{2.5}$ and PM_{10} levels and their spatial distribution throughout the year Arkouli et al. (2010). Our investigation contributes new information regarding both the daily and seasonal patterns of hourly *EBC* concentrations, identifying the contributions of primary permanent emission sources as well as local and regional sources that are likely to impact the urban atmosphere on an intermittent basis. Section 2 presents the observational data analyzed and discusses our methods for correcting and disaggregating BC concentrations. Section 3 addresses results for total BC concentrations and estimates of biomass burning and fossil fuel combustion contributions to total *EBC* levels. Finally, Section 4 presents the main conclusions of this investigation.

2. Data and methods

2.1. Measurement site

The MABA is located on the southern shore of the La Plata River on a flat plain, and is Argentina's only megalopolis, with a population of approximately 13 million, a population density of 4600 inhabitants per km^{-2} and ca. 4.1 million vehicles registered reported by the National Vehicle Registration Directory (DNRPA). The MABA is composed of the city itself and 24 surrounding districts, and is characterized by social and territorial inequities (INDEC, 2017).

The MABA exhibits marked seasonal climatological variation as a result of the influence of semi-permanent systems, including the subtropical South Atlantic Anticyclone (SAA) and synoptic and mesoscale events such as fronts and convective storms (Garreaud and Falvey, 2008). The climate is humid-temperate with mean annual precipitation of 1200 mm, concentrated mainly in summer and mean annual temperature of 17.9 °C (period 1981-2010). Winds derive predominately from the north and northeast as a result of the influence of the SAA and the city's coastal location (Barros et al., 2006). The annual precipitation for the sampling period was near normal. However, the rainfall pattern showed monthly variability. Some months exceeded the historic values (November 2014 and August 2015) and other months presented smaller values than the historic deficits and lower number of days with precipitation than normal (March 2015). In general, the temperature remained close to the climatic values, nevertheless, winter 2015 was warmer than average. During the monitoring campaign, mean wind speed was 2.5 m/s, rarely exceeding 12 m/s, slightly lower than normal conditions but higher than mean minimum. Predominant wind direction was north-northeast, except during winter when it shifted to north-northwest.

Monitoring was carried out for an open area (34.56°S, 58.51°W, 20m asl) situated 14 km away from the city center and influenced by the emissions of both mobile and stationary combustion sources (Fig. 1). It is worth noting that emission control has been poorly enforced within the MABA, particularly for buses and light duty trucks. Characteristics of the three main roadways are presented in Table 1.

A park was located to the east of the sampling site. Residential areas of different socio-economical levels were located in the other directions; most households used natural gas for heating and cooking and charcoal and wood for barbecuing throughout the year; some houses occasionally used wood stoves during winter. LPG was used for cooking in a low-income area to the southwest; open wood fires occurred

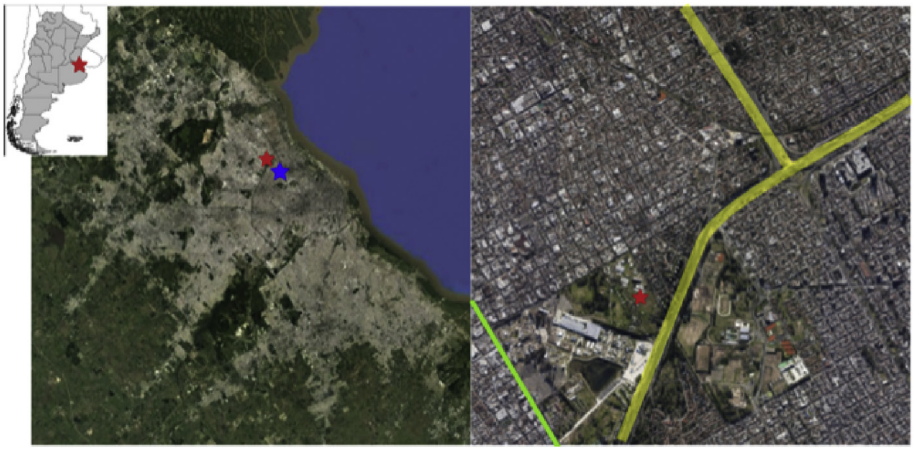

Fig. 1. Map of the study area (left) and surroundings (right). Stars represent the monitoring site (red) and the meteorological station (blue) and lines (yellow) the two main highways and the avenue of the area (H1 and H2 in yellow and A1 in green). Their main characteristics are provided in Table 1. (For interpretation of the references to color in this figure legend, the reader is referred to the Web version of this article.)

Table 1
Summary of main roads, location and fleet.

Label	Name	Distance from the Site	AADT	Description of the fleet
H1	Gral Paz, Avenue	250 m E	195	passenger cars, buses and light duty trucks (LDT)
H2	Panamericana, Highway	1.6 km N	375	passenger cars, buses, LDT and heavy duty trucks
A1	De Los Constituyentes, Avenue	1.3 km S		vehicles including old HDT and buses circulate at relatively low speed in a stop-and-go pattern.

AADT: annual average daily traffic (in thousand of vehicles). Reported by the local governmental sources in 2015.
Passenger cars use gasoline, diesel and compressed natural gas (CNG), LDT diesel and CNG and HDT only diesel.

sporadically in this area.

2.2. Instrument

A 7-wavelength Aethalometer (Magee Scientific USA, Model A42, λ= 370, 470, 520, 590, 660, 880 and 950 nm) equipped with a $PM_{2.5}$ cut-off size inlet was used at a flow rate of 4.90 l/min. *EBC* concentrations were determined at successive 5-min intervals by measuring optical attenuation (ATN) caused by $PM_{2.5}$ deposited on a roll of quartz fiber filter tape. The Aethalometer automatically advances the tape to provide a fresh filtration spot before carbon aerosol loading becomes greater than a pre-set limit for the ATN value; this value was set at 75 units for any of the seven wavelengths, in accordance with the manufacturer's recommendations. Advancing the filter tape takes 15 min, during which no measurements are performed. In an urban environment, the tape may advance three or four times per day.

Spot optical attenuation was calculated based on light intensity transmitted through the blank filter (I_0) and through the deposited particles (I) using the Beer-Lambert law (Equation (1)).

$$ATN \equiv \ln\left(\frac{I_0}{I}\right)*100 \tag{1}$$

The aerosol attenuation coefficient for sampled particles (b_{ATN}) was calculated using the change in light attenuation as a function of time, the volumetric flow rate Q, and the filter spot area A (1.67 cm^2):

$$b_{ATN} = \frac{A}{Q}\frac{\Delta ATN}{\Delta t} \tag{2}$$

EBC concentrations for sampled airflow were estimated based on the rate of change in ATN between two successive measurements resulting from the accumulation of optically absorbing particles on the filter (Park et al., 2010). Measurements at $\lambda = 880nm$ were used to calculate *EBC* concentrations, given that BC absorbs efficiently in the IR spectra and this band has been reported to be in better agreement with BC measured by thermal-optical reflectance methods (Lin et al., 2014). Biomass burning and traffic contributions were estimated using measurements at 470 nm and 950 nm wavelengths, respectively, as specified in Section 2.5.

2.3. Data corrections and processing

Previous studies indicate that Aethalomether measurements are affected by multiple factors: i) noise due to small, random fluctuations of digitized signals, ii) signal drift as a result of incremental particle load on the filter, and iii) multiple scattering by the fiber's filter. Attenuation is expected to increase as the load on the filter spot increases; however, deviations from this monotonic relationship often result from electronic noise. Since b_{ATN} calculations are made for successive differences of ATN, artificially negative values could appear and should be corrected (Hagler et al., 2011).

To reduce signal noise, a post-processing strategy was applied: (i) spots that did not fulfill the monotonic increasing condition were identified, (ii) for these spots, raw values were replaced by the 30-min moving average. An additional correction was applied to address the fact that BC measurements decrease with increasing filter loading but are enhanced by multiple scattering, which increases the optical path. Different methods for correcting for these effects have been proposed and widely applied (Drinovec et al., 2015; Herich et al., 2011; Sandradewi et al., 2008a). A group of these methods, proposed by Schmid et al. (2005) and Collaud Coen et al. (2010), require complementary measurements such as scattering coefficients or BC mass concentrations. In this study, such equipment was not available and the empirical correction described by Weingartner et al. (2003) was therefore applied, as suggested by Collaud Coen et al. (2010). This algorithm uses two calibration factors, C and R (ATN), to address multiple scattering and shadowing effects, respectively (Equation (3)), and therefore convert Aethalometer attenuation measurements to absorption coefficients.

$$b_{abs} = b_{ATN}\frac{1}{C.\,R(ATN)} \tag{3}$$

These factors describe two effects that alter the optical properties of particles embedded in the filter with respect to the properties of the same particles in their airborne state. The constant C, taken as 2.14 (Drinovec et al., 2015; Weingartner et al., 2003), compensates for multiple scattering of light beams by the filter fibers in the unloaded filter; R (ATN) describes the shadowing effects caused by deposited particles (Favez et al., 2009).

$$R(ATN) = \left(\frac{1}{f} - 1\right)\frac{ln(ATN) - ln(10)}{ln(50) - ln(10)} + 1 \tag{4}$$

In Equation (4), f is used as a parameter to compensate the instrumental error that occurs when the shadowing effect is disregarded. We obtained our f value by minimizing the discontinuities in b_{ATN} for each wavelength before and after changing the filter spot, resulting in $f_1 = 1.22$, $f_2 = 1.15$, $f_3 = 1.12$, $f_4 = 1.10$, $f_5 = 1.08$, $f_6 = 1.04$, $f_7 = 1.02$.*EBC* concentrations were calculated as follows:

$$EBC\,[g/m^3] = \frac{b_{abs}}{\sigma_{abs}} = \frac{b_{ATN}}{\sigma_{ATN}R(ATN)} \;\; with \;\; \sigma_{ATN} = \sigma_{abs}C \tag{5}$$

where σ_{abs} is the mass absorption cross-sections and σ_{ATN} is the aerosol light attenuation cross-section. Values for σ_{ATN} of 31.1, 16.6 and 15.4 m^2/g for 470, 880 and 950 nm wavelengths, respectively, were recommended by the manufacturer and widely applied in the literature and were therefore selected for this study (Fuller et al., 2014; Sandradewi et al., 2008a; Segura et al., 2014). These values are consistent with σ_{abs} reported for similar conditions, from 7.3 to 8.8 m^2/g (Zanatta et al., 2016; Laborde et al., 2013).

2.4. Other air pollution and meteorological data

The Buenos Aires SPARTAN network station (Snider et al., 2015) is located less than 50 m away from the Aethalometer. *BC* and $PM_{2.5}$ concentrations reported by this network were used to calculate the corresponding ratio and to complement Aethalometer measurements.

For biomass burning events, active fire locations from the Fire Information for Resource Management System (FIRMS) MCD14ML fire database (available on-line at https://earthdata.nasa.gov/active-fire-data) were used to determine air masses reaching the city from areas where hot spots were registered. This approach was complemented

using a Cloud-Aerosol Lidar with an Orthogonal Polarization (CALIOP) instrument on board the Cloud-Aerosol Lidar and Infrared Pathfinder Satellite Observation (CALIPSO) spacecraft, which measures vertical profiles of 532 nm total attenuated backscatter and provides data for aerosol subtypes (Omar et al., 2009; Young and Vaughan, 2009). Wind direction (standard 16 compass directions) and wind speed hourly data of the Buenos Aires Observatory (34.58°S, 58.48°W, 25m asl), was provided by the National Weather Service of Argentina (SMN), located 5 km away from the measurement site. Data from this station can be considered representative of air ow over the city.

In addition to surface data, the SMN reports (i) daily upper air temperature profiles from radiosonde at 12 GTM and (ii) convective mixing heights values estimated as the top of the layer where the temperature gradient is close to the dry adiabatic lapse rate. We estimated hourly convective mixing height from surface meteorological data using the largest value between convective (Z_c) and mechanical (Z_m) mixing heights for daytime conditions, and the mechanical mixing height for the night. Z_m values were obtained from the well-known Equation (6), where u_* corresponds to the friction velocity and f is the Coriolis parameter, while Z_c were calculated solving Equation (7) proposed by Batchvarova and Gryning (1991).

$$Z_M = \frac{u_*}{4.f} \tag{6}$$

$$\frac{dZ_c}{dt} = (1 + 2.A)\frac{H}{\rho.\ C_P.\ \gamma_\theta.\ Z_C} + 2.B.\ \frac{u_*^3.\ T}{g.\ \gamma_\theta.\ Z_C^2} \tag{7}$$

where H, is the surface heat flux, ρ the density of the air, C_P the specific heat of air at constant pressure, γ_θ the potential temperature gradient above the mixing height, T is the reference temperature (2 m above the surface), g the acceleration of gravity. A and B are parametrization constants. This differential equation was numerically solved, using the approach described in Turtos Carbonell et al. (2010) with A = 0.2 and B = 5.0. The results for 12 GTM were compared with the values reported by the SMN for the period 2001 2010 and a Pearson correlation coefficient of 0.798 was obtained.

2.5. Source attribution methodology

2.5.1. Equivalent BC concentrations from fossil fuel combustion and biomass burning

We addressed the relative contribution of biomass burning and fossil fuel based on measured 470 nm and near-infra-red (IR1: 950 nm) absorption signals, assuming negligible apportionment from all other sources:

$$EBC = EBC_{bb} + EBC_{ff} \tag{8}$$

where *bb* and *ff* stands for biomass burning and fossil fuels, respectively, and

$$b_{abs}(\lambda) = b_{abs,bb}(\lambda) + b_{abs,ff}(\lambda)\ for\ \lambda = 470nm, 950nm \tag{9}$$

where b_{abs} are the absorption coefficients.

The relation between the absorption coefficients and the Ångström exponents for those bands (equation (10)) was used to calculate the α experimental values for the whole monitoring campaign, and similar expressions was used to estimate EBC_{ff} and EBC_{bb} (equations (11) and (12)).

$$\frac{b_{abs,470nm}}{b_{abs,950nm}} = \left(\frac{470nm}{950nm}\right)^{-\alpha} \tag{10}$$

$$\frac{b_{abs,ff,470nm}}{b_{abs,ff,950nm}} = \left(\frac{470nm}{950nm}\right)^{-\alpha_{ff}} \tag{11}$$

$$\frac{b_{abs,bb,470nm}}{b_{abs,bb,950nm}} = \left(\frac{470nm}{950nm}\right)^{-\alpha_{bb}} \tag{12}$$

Since there were no auxiliary measurements that allowed calculating Ångström exponents for pure fossil fuel and pure biomass burning, values reported in other studies were explored. There is a general agreement about the value of α for pure fossil fuel and therefore it was set as 1.1 (Sandradewi et al., 2008b; Fuller et al., 2014). For biomass burning a larger range of values is reported, depending on the type of biomass and the combustion efficiency (Favez et al., 2010): sources burned under smoldering conditions, such as leaf litter or charcoal used in grill cooking, are associated with α_{bb} values greater than 2 while sources burned under flaming conditions consistent with wheat-residue-burning plumes with values lower than 1.4 (Garg et al., 2016). In this work a range from 1.5 to 2.6 was explored for α_{bb}.

(Sandradewi et al., 2008b; Fuller et al., 2014), for biomass burning a larger range of values is reported, depending on the type of biomass and the combustion efficiency (Favez et al., 2010): sources burned under smoldering conditions, such as leaf litter or charcoal used in grill cooking, are associated with α_{bb} values greater than 2 while sources burned under flaming conditions consistent with wheat-residue-burning plumes with values lower than 1.4 (Garg et al., 2016). In this work a range from 1.5 to 2.6 was explored for α_{bb}.

EBC_{ff} and EBC_{bb} were calculated with $b_{abs,ff}(950nm)$ from Eqs. (8) to 12), $b_{abs,ff}(950\,nm)$ was determined and EBC_{ff} and EBC_{bb} were calculated as

$$EBC_{ff} = EBC\frac{b_{abs,ff}(950nm)}{b_{abs}(950nm)} \tag{13}$$

$$EBC_{bb} = EBC - EBC_{ff} \tag{14}$$

2.5.2. Spatial and temporal patterns of the black carbon contributing sources

The time series of determined *EBC* concentrations, together with those of their estimated components (EBC_{ff} and EBC_{bb}) and variations in meteorological conditions, were used to infer temporal and spatial variability in emissions contributions from biomass burning and fossil fuel combustion. We employed univariate analysis (i.e. mean, median, 25^{th} and 75^{th} percentile, minimum and maximum) and bivariate polar plots to determine different source types through wind speed dependence, discriminated by wind direction. High concentrations under low wind speeds ($<3m/s$) are indicative of surface emissions released with little or no buoyancy, whereas high concentrations at high wind speeds ($>6m/s$) are indicative of stack emissions or emissions at high velocity and/or at a greater distance (Uria-tellaetxe and Carslaw, 2014).

Primary regional sources of emissions have been identified using the potential source contribution function (PSCF) (Dos Santos et al., 2012; Polissar et al., 2001; Zha et al., 2014). Three-day backward air mass trajectories were calculated for every 6 h, using the hybrid single-particle Lagrangian integrated trajectory (HYSPLIT) model (Draxler and Hess, 1998) with NCEP-NCAR Reanalysis meteorological data (Kalnay et al., 1996; Kistler et al., 1999) and arrival heights at the receptor location setting of 100, 500 and 1000 m. PSCF was calculated on a 0.5 × 0.5 resolution grid that covered the area from 25-45S and 45-80W, using the 75th percentile as the criterion value. These results were weighed by an arbitrary function (W_{ij}) to better reflect uncertainty in values for cells with a smaller number of trajectories (Polissar et al., 2001):

$$WPSCF_{ij} = \frac{m_{ij}}{n_{ij}}W_{ij} \tag{15}$$

$$W_{ij} = \begin{cases} 1, & n > 2\overline{n} \\ 0.75, & \overline{n} < n \le 2\overline{n} \\ 0.5, & 0.5\overline{n} < n \le \overline{n} \\ 0.15, & n \le 0.5\overline{n} \end{cases} \tag{16}$$

where n_{ij} is the number of endpoints that cross the ij_{th} cell, $\overline{n}$ is the average number of endpoints that cross a cell, m_{ij} is the number of

endpoints for the same cell which are associated with a *EBC* concentration higher than the criterion defined, and WPSCF is the weighted PSCF.

2.5.3. Extreme EBC_{bb} concentration events

In the analysis of the EBC_{bb} concentration time series, we noted that there were few occasions when extremely high EBC_{bb} levels persisted for several hours, and we therefore deemed valuable an exploration of the circumstances surrounding these events. EBC_{bb} concentrations above the 99^{th} percentile were grouped by date and classified considering the ventilation coefficient (VC) defined as the product of the planetary boundary layer height (PBLH) and average wind speed through the mixing layer (Arkouli et al., 2010). One-hour isolated records were not taken into consideration. The ventilation coefficient is a good indicator of the potential dispersion of pollutants in the atmosphere, with lower values corresponding to higher concentrations, independent of the apportionment of the different sources.

All of the events for which high concentrations of EBC_{bb} were registered together with low ventilation conditions (zero or near zero ventilation coefficients) were postulated as local extreme biomass burning events, while under different ventilation conditions these were postulated as regional extreme biomass burning events, as described in the flow chart presented in Fig. 2.

For postulated local events, we verified whether high BC local emissions for a particular event and/or a cold air intrusion leading to extreme temperature lows had occurred. For regional events, we reviewed whether air masses arriving in the city during the same period crossed fire regions, using the FIRMS database combined with HYSPLIT back-trajectories. To complement this analysis, CALIOP Data v3.3 was used to confirm the presence of smoke aerosols.

3. Results

3.1. Temporal variations of EBC concentrations

Hourly averages for *EBC* concentrations exhibited a log-normal distribution, confirmed with a 99% level of confidence, with a mean of 3.18 $\mu g/m^3$ and a median of 2.03 $\mu g/m^3$. The 25^{th} and 75^{th} percentiles

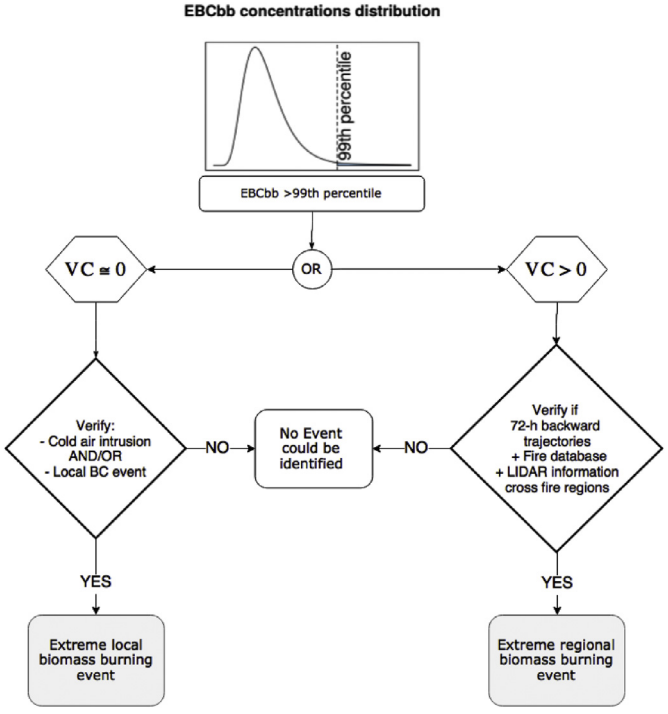

Fig. 2. Flow diagram of extreme EBC_{bb} events identification methodology.

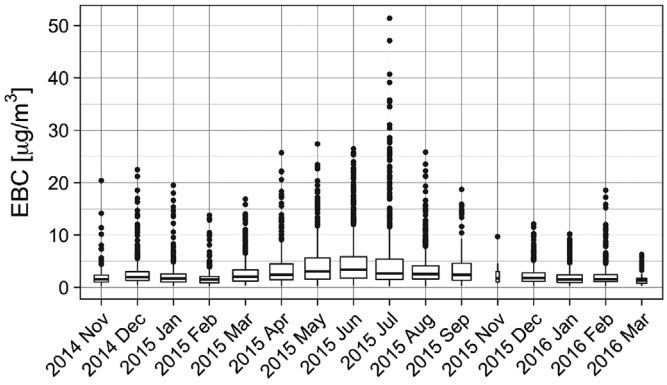

Fig. 3. Monthly variation of hourly *EBC* concentrations. The symbols, vertical line, lower whisker, lower edge of the box, central line of the box, upper edge of the box, upper whiskers, are standard deviation, 5^{th} percentile, 25^{th} percentile, median, 75^{th} percentile and 95^{th} percentile, respectively. Box width is proportional to the square root of the number of observations in each month.

were calculated as 1.23 and 3.57 $\mu g/m^3$ and the 5^{th} and 95^{th} percentiles were 0.58 and 9.42 $\mu g/m^3$ respectively. Average *EBC* levels are similar to those reported for other Latin American cities (Carbone et al., 2013; Gramsch et al., 2016; Seguel et al., 2009; Souto-Oliveira et al., 2016).

EBC exhibited a well-defined diurnal and seasonal cycle. The diurnal cycle during weekdays was clearly governed by traffic patterns, following a typical bimodal distribution explained in detail in Section 3.3.

Hourly concentrations were maximum during winter (June-July-August) (Fig. 3). During this period 24-h average concentrations reached values of 22 $\mu g/m^3$. Although maximum values for BC have not yet been established in terms of air quality or health, the associated $PM_{2.5}$ concentrations considering the average $EBC/PM_{2.5}$ ratio calculated from SPARTAN data of 0.16, exceeded the maximum recommended for $PM_{2.5}$ (25 $\mu g/m^3$) by the WHO. Therefore other campaigns should be carried out in the area that include other criteria pollutants such as CO, NO_x and $PM_{2.5}$ to evaluate in detail the air quality of the area.

Diurnal cycle during summer (January-February-March) exhibited comparatively lower values within a narrower spread.

When *EBC* mass concentrations were examined by season, we observed higher values during winter nights that could be related to a combination of heating emissions and lower and more stable PBLH; flatter patterns were observed during summer and rainy seasons.

Our results demonstrate that in Buenos Aires, *EBC* concentrations are similar to those measured in other Latin American cities. Black carbon is normally a substantial fraction (20-30%) of $PM_{2.5}$ (Begum et al., 2012; de Miranda et al., 2012; Seguel A. et al., 2009). $EBC/PM_{2.5}$ ratios estimated using data from the SPARTAN network fell within the regional range of $0.09 - 0.36$, with a median value of 0.15. These fractions corresponded only to the summer, during which data from the SPARTAN network were available; they are expected to vary in winter due to source seasonality.

3.2. Selection of ångström exponents

The experimental values of the total Ångström exponents obtained, using the expression showed in equation (10), presents a median of 1.1 with a range from 1.05 to 1.17, corresponding to the 25^{th} and 75^{th} percentiles, totally in line with the values reported for fossil fuel combustion sources. This result is consistent with the expected significant role of the on-road mobile sources in this urban area.

For the selection of the Ångström exponent for pure biomass burning a range of 1.5–2.6 was explored. In the range 1.5–1.9 a high proportion of situations with $EBC_{ff} = 0$ was obtained, even during rush hours, when it is well known the high traffic flow in the area. For this

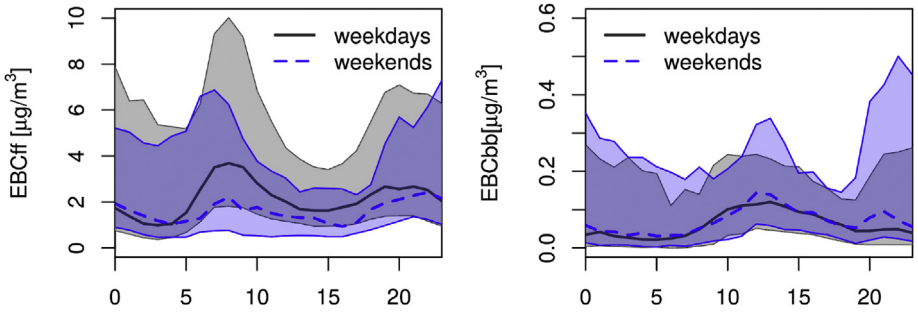

Fig. 4. Diurnal cycle of *EBC* biomass burning and fossil fuel concentrations for weekdays and weekends. Shaded areas represent concentrations between 25^{th} and 75^{th} percentile.

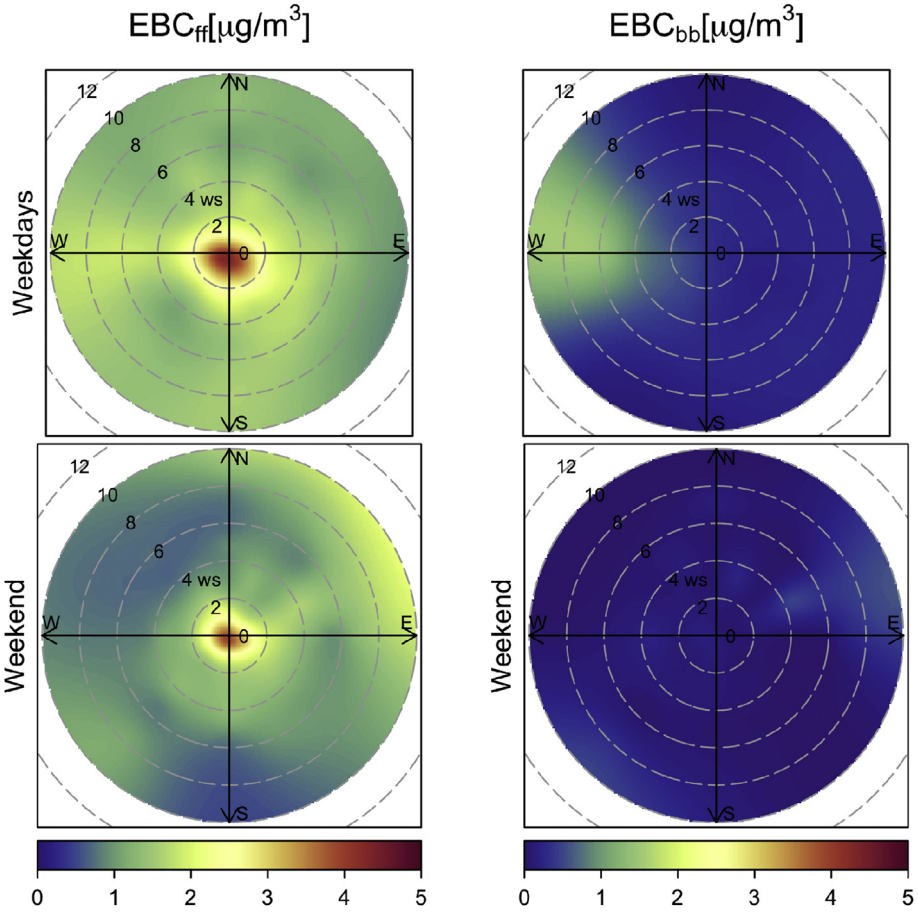

Fig. 5. Bivariate polar plot of *EBC* fossil fuel and biomass burning hourly median concentrations by wind speed and direction for weekdays and weekends. The color scale shows the concentration of EBC_{ff} and EBC_{bb} in $\mu g/m^3$ and the radial scale shows the wind speed, which increases from the center of the plot radially out-wards.

reason a range of 2–2.6 was considered as plausible, and the median EBC_{ff} and EBC_{bb} concentrations of the range considered were reported in this study. These levels correspond to α_{bb} of 2.2 which is consistent with biomass burning under smoldering conditions (Garg et al., 2016). Charcoal burning for grilling purposes used in grill cooking corresponds to α_{bb} greater than 2.0 being this the most frequent source of local biomass burning. These levels correspond to α_{bb} of 2.2, in line with biomass burning under smoldering conditions (Garg et al., 2016), which is consistent with those of the combustion of charcoal for grilling purposes, the most frequent source of local biomass burning in the area.

The uncertainty associated with the selection of Ångström exponents resulted 0.02 $\mu g/m^3$ for both fossil fuel and biomass burning. It was estimated using the selected ranges of α_{ff} y α_{bb} in the calculation of EBC_{ff} and EBC_{bb}. In relative terms these uncertainties values represent less than 2% for the median of EBC_{ff} and about 30% for the median of EBC_{bb}.

3.3. Biomass burning and fossil fuel contributions

Fig. 4 displays *EBC* fossil fuel and biomass burning daily patterns during weekdays and weekends. During weekdays, the EBC_{ff} median value was 2.13 $\mu g/m^3$ and the values corresponding to the 1^{st} and 3^{rd} quantile were 1.30 and 3.81 $\mu g/m^3$ during weekends, these decrease to 1.60, 0.91 and 2.86 respectively. The diurnal cycle of EBC_{ff} during working days showed a distinctive peak at 8 a.m., an absolute minimum at about 3 p.m. and a relative maximum beginning at 6 p.m., after which concentrations remained at a fairly constant level until about 9 p.m. Weekend patterns were flatter, presenting higher values at about midnight. EBC_{bb} median, 1^{st} and 3^{rd} values were $5.9\ 10^{-2}$, $2.1\ 10^{-2}$ and $1.2\ 10^{-1}$ $\mu g/m^3$ during weekdays and $7.0\ 10^{-2}$, $2.8\ 10^{-2}$ and $1.5\ 10^{-1}$ $\mu g/m^3$ during weekends. The diurnal cycle displayed two maximums, at noon and at night, with more distinctive peaks on weekend days. These relatively higher levels may be associated with residential emissions of

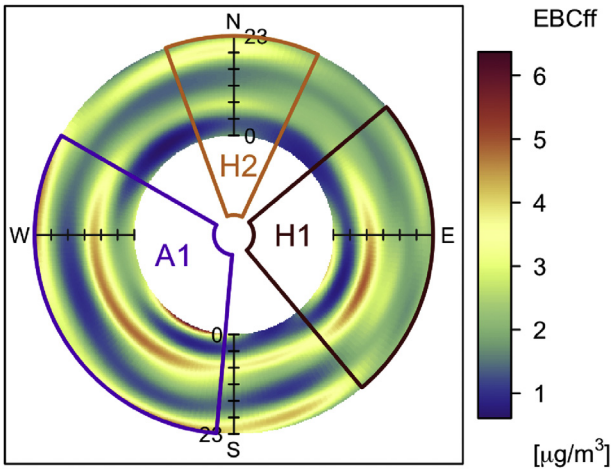

Fig. 6. Polar annulus plots for hourly median EBC_{ff} concentrations, by hour of day, with the earliest time (0:00) shown in the inner circle and the latest time (23:00) at the outer circle. All units are in $\mu g/m^3$. The circular sectors represent the directions influenced by the main traffic areas, as defined in Table 1 and Fig. 1: A1 (violet), H1 (dark red) and H2 (orange).

Table 2
Summary of median, 25^{th} and 75^{th} percentiles of EBC, EBC_{ff} and EBC_{bb} for the entire period and by season.

	Campaign	Winter (JJA)	Summer (DJF)	Autumn (MAM)	Spring (SON)
EBC_{ff}	2.03 (1.23-3.57)	2.77 (1.61-5.19)	1.65 (1.06-2.60)	2.30 (1.33-4.25)	2.00 (1.19-3.43)
EBC_{bb}	1.98 (1.17-3.53)	2.66 (1.48-5.04)	1.62 (1.03-2.59)	2.28 (1.27-4.21)	1.84 (1.10-3.29)
	0.06 (0.02-0.13)	0.10 (0.05-0.22)	0.04 (0.01-0.09)	0.06 (0.02-0.13)	0.08 (0.03-0.20)

Units.$\mu g/m^3$

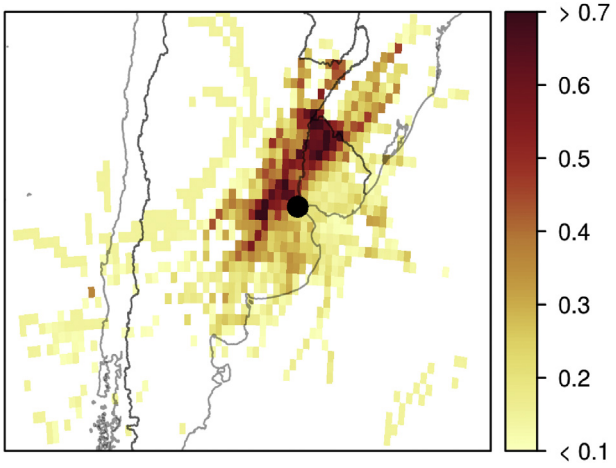

Fig. 7. WPSCF of the EBC_{bb} above the 75^{th} percentile for the entire period with the receptor at 100 m.

charcoal combustion from grilling. The diurnal cycle of EBC for working days exhibited the same shape as EBC_{ff}; this behavior together with the relative contribution of EBC_{ff} and EBC_{bb} to the total concentration of EBC confirmed that fossil fuel emissions dominated total EBC concentrations. On average, EBC_{ff} represented 96% of the total EBC measured consistently and with proximity to high traffic highways.

Fig. 5 exhibits the bivariate polar plot of median concentrations of EBC_{ff} and EBC_{bb} by wind speed and direction. The color scale represents

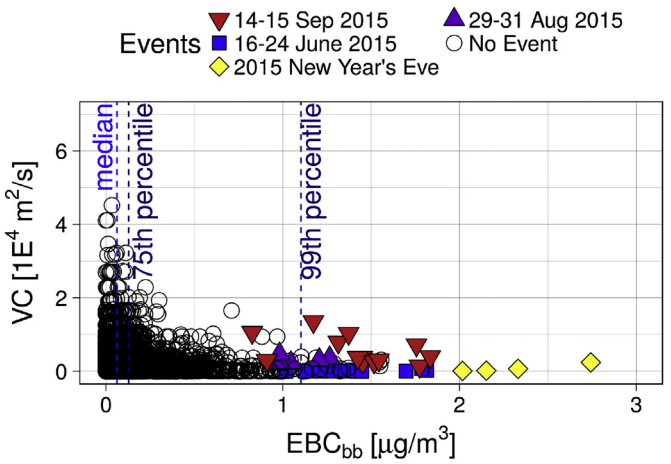

Fig. 8. Scatter plot for EBC_{bb} concentrations and the ventilation coefficients for the entire period. Local and regional events are in blue and yellow and violet and red respectively. Vertical lines represent media and 75^{th} percentile values. (For interpretation of the references to color in this figure legend, the reader is referred to the Web version of this article.)

the concentration and the radius increasing wind speed. EBC_{ff} presented a rather uniform distribution with wind direction, particularly for weekdays, denoted by the very similar color distribution in the four quadrants; during weekends, the sector W-NW and WSW-ESE exhibited relatively lower concentrations at wind speed larger than 6 m/s. Decreasing EBC_{ff} levels with wind speed were noticeable for both weekdays and weekends; concentrations decreased sharply within the range 0–3 m/s. EBC_{bb} exhibited also a rather uniform distribution at the low end of the concentration scale with the noticeable exception of the area of relatively high concentrations in the WNW-WSW sector at wind speeds over 4 m/s. We further analyzed the occurrence of these values and identified that they largely belong to the extreme EBC_{bb} concentrations events discussed in Section 3.4, which were superimposed on local contributions. The relatively high levels of EBC_{bb} shown in Fig. 5 occurred under the least frequent wind directions. These were not the only extreme EBC_{bb} events identified; however high EBC_{bb} levels corresponding to other events did not appear in this figure; since they occurred under more frequent directions, they did not impact the median EBC_{bb}, which was dominated by numerous lower values.

Fig. 6 is a polar annulus plot representing hourly variations by wind direction of the median EBC_{ff} concentrations. Moving across the annulus depicts concentrations through the hour of the day, from the inner part representing the median value for 0:00 and the outer part the median value for 23:00. The areas of influence for the primary mobile sources A1, H1 and H2 are delimited in violet, orange and burgundy respectively for better understanding how the different sources affected the site. The bimodal pattern of the diurnal cycles depicted in Fig. 4 can be also appreciated in Fig. 6, by the two relatively higher concentration annuli, typically occurring in the 8-12 and 20-24 intervals. The shape and the coverage of these two annuli are not homogeneous throughout wind direction, indicative of the different pattern of the contributing sources. Maximum median concentrations (in the range 3.5–5.2 $\mu g/m^3$) were registered in the sectors under the influence of A1 and H1, from 8:00 to 12:00. This may be attributable to the contribution of emissions from the morning traffic peak of these roads, which are typically busiest in the morning of weekdays, delivering traffic from suburban to urban areas. Lower concentration levels registered during the afternoon were most likely consequence of decreasing traffic flow and higher convective mixing heights. Since H1 is closer to the monitoring site and registers larger traffic flow, we expected that the EBC_{ff} concentrations under winds connecting H1 with the monitoring site would have been higher than those concentrations from A1. However, this was not the case. It is plausible to attribute this behavior to the following facts: (i)

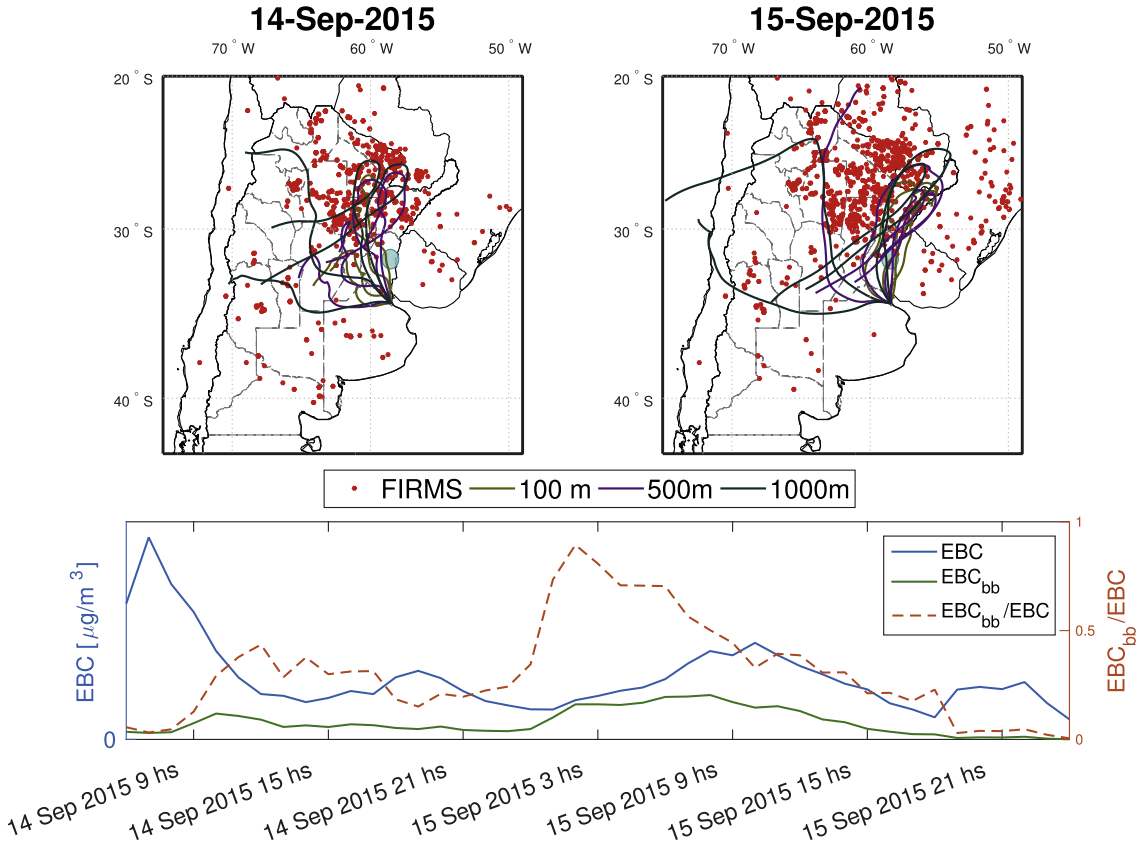

Fig. 9. Regional Event: (up) Active fire locations during three-day backward trajectories arriving every 6 h at the sampling site at 100, 500 and 1000m and (down) Time Series of hourly *EBC* and EBC_{bb} concentrations for September 14^{th}-15^{th} 2015. Light blue circle represents the area of El Palmar where the controlled fires took place. (For interpretation of the references to color in this figure legend, the reader is referred to the Web version of this article.)

the numbers of heavy-duty diesel vehicles, well-known major black carbon emitters (Bond et al., 2013), is typically much larger in A1 than in H1, (ii) the average speed is higher in H1, and (iii) the number of flowing traffic stops is higher in A1. In general, concentrations were lower when winds came from the H2 direction as compared to the other two sources. Two possible explanations for the relatively low concentrations of the highly trafficked H2 include: (i) the relatively lower emissions associated with the high-speed pattern, and (ii) the significant distance to the monitoring point.

Concentration levels of *EBC*, EBC_{ff} and EBC_{bb} organized by seasons are reported in Table 2, where can be observed greater concentration levels in winter than in summer for all of them. This difference is dominated by the contribution from fossil fuels. Traffic and thermal power plants were the only black carbon sources exhibiting seasonal variations in MABA during the monitoring period. It is worth noticing that: (i) the contribution of thermal power plants can be considered negligible at the monitoring site (Reich et al., 2006), and (ii) liquid fuels are not customarily used for household heating, which is based on natural gas and electricity. The sole increase in traffic flow during winter cannot explain the increased level of EBC concentration. We postulate that the other contributing factor is the lower PBLH during winter, which worsen air pollutant dispersion.

We estimated the WPSCF for the set of EBC_{bb} values above the 75^{th} percentile. The results are shown in Fig. 7 and indicate that the highest WPSCF values were located in an area S-W and N-E of the monitoring point, which includes central-east Argentina, north-west Uruguay, southern Brazil and the northern portion of the Buenos Aires province. Intensive agricultural and forestry activities take place within this region and it is therefore plausible to associate these high EBC_{bb} levels with biomass burning emissions transported from this region to the monitoring site by N-NE winds. These results are consistent with those presented in Fig. 5 and associated with regional biomass burning areas.

3.4. Periods of extreme EBC_{bb} events

Concentrations of EBC_{bb} above the 99^{th} percentile were grouped by date and classified considering the ventilation coefficient, ambient temperature and specific circumstances related to high emissions. Using the procedure discussed in Section 2.5.3, two events with near-zero VC occurred from June 17^{th}-23^{rd} 2015 and December 31^{st} 2014-January 1^{st} 2015, and two events with VC higher than zero (August 30^{th}-31^{st} and September 14^{th}-15^{th} 2015) were identified (Fig. 8).

From June 17^{th}-23^{rd} 2015, the biomass burning contribution reached values of 44% of total registered *EBC*. During this period, very cold air covered the entire territory and produced very low temperatures and increased domestic heating requirements. These two conditions, together with calm wind conditions, increased the level of biomass contribution significantly, almost triplicating average EBC_{bb} and confirming this extreme biomass burning event as local in origin.

The highest EBC_{bb} concentrations were measured during the summer days of December 31^{st} 2014 and January 1^{st} 2015 under stable conditions. It could be tempting to assign these situations to the usual increase in the use of charcoal for New Year's Eve barbecues, but the simultaneous use of fireworks, which typically contain carbonaceous materials (black carbon, sugar or starch) must also be considered, as argued by Yerramsetti et al. (2013). This particular BC event occurred under calm conditions and could also be classified as locally driven.

The two situations identified with VC greater than zero were verified using the FIRMS database combined with HYSPLIT back-trajectories to confirm that air masses arriving in the city during these periods crossed through fire regions. CALIOP Data v3.3 was used to complement this analysis, demonstrating the presence of smoke aerosols from

the surface up to a height of 3 km. Under these circumstances, the EBC_{bb} concentration estimated from our measurements fell between three and six times the average levels for the entire period, and was unexplained by any specific local biomass burning event. For all of these reasons, we assigned these atypically high EBC_{bb} concentrations to regional sources.

Fig. 9 shows the temporal evolution of *EBC* and EBC_{bb} for the September $14^{th} - 15^{th}$ event. During this period, the EBC_{bb}/EBC ratio was higher than 50% for 10 consecutive hours, including morning rush hour on November 15^{th}. On these dates, controlled fires were reported by local media in the area of El Palmar de Colón, located within the range of WPSCF values greater than 0.5 (El Entre Ríos, 2015).

In order to verify the proposed methodology, all back-trajectories were analyzed for the 17 months of study, and an additional instance was identified when air trajectories arriving in the city had crossed fire regions (August 6^{th} and 9^{th}, 2015). Unfortunately, the Aethalometer was not operational during this event.

4. Conclusions

Diurnal, monthly and seasonal variations of *EBC* concentrations in the Metropolitan Area of Buenos Aires were analyzed over a 17-month period, using 880 nm wavelength Aethalometer data with corrections for filter overloading, multiple scattering, and signal noise. The information obtained by the 479 and 950 nm bands was useful for identifying fossil fuel and biomass burning apportionment. We also discriminated between local and regional sources using a combination of local wind speed and direction, back-trajectory air masses and satellite fire data. To the best of our knowledge, this is the first study reporting BC concentrations at hourly resolution for the 13^{th} Megalopolis of the world.

It was verified that the city's own emissions define both daily and seasonal variations and constitute the primary source of EBC. Like in other large urban conglomerates, emissions from diesel vehicles resulted the largest black carbon contributor; the contribution of the use of charcoal and wood for cooking and the combustion of wood and other biomass for heating during winter is far less significant. Despite the limited occurrence of regional events affecting MABA atmospheric conditions, these sources (biomass burning from agricultural and forestry activities) are relevant due to the significant distance from the urban area and their relative contribution to *EBC* that can exceed 50% on such occasions.

The results obtained in this study demonstrate the ability of applied methods to identify sources related to vehicle emissions and biomass burning. The type of analysis used in this study, with the addition of simultaneous $PM_{2.5}$ measurements, can serve as a verification tool for local emissions inventories. Complementary studies should be carried out to generate reference measurements of black carbon with thermal methods or scattering coefficients in order to reduce the uncertainties surrounding the role of fossil fuel and biomass burning.

Acknowledgments

Financial support is acknowledged from FONDAP-CR2 15110009 (CONICYT, Chile), and grant PICT 2016-3590 (ANPCyT, Argentina). The authors would like to thank the CITEDEF LIDAR division for allowing us to safely locate our monitoring equipment. We acknowledge the use of data and imagery from LANCE FIRMS operated by the NASA/GSFC/Earth Science Data and Information System (ESDIS) with funding provided by NASA/HQ, CALIOP data obtained from the NASA Langley Research Center Atmospheric Science Data Center, and meteorological data provided by the National Weather Service of Argentina. Laura Gallardo acknowledges FONDAP 15110009 and FONDECYT 1150873.

References

Arkouli, M., Ulke, A.G., Endlicher, W., Baumbach, G., Schultz, E., Vogt, U., Müller, M., Dawidowski, L., Faggi, A., Wolf-benning, U., Scheffknecht, G., 2010. Distribution and temporal behavior of particulate matter over the urban area of Buenos Aires. Atmos. Pollut. Res. 1 (1), 1–8. www.atmospolres.com.

Barros, V., Clarke, R., Silvia Dias, P., 2006. Climate Change in the La Plata Basin.

Batchvarova, E., Gryning, S.-E., Aug 1991. Applied model for the growth of the daytime mixed layer. Boundary-Layer Meteorol. 56 (3), 261–274. https://doi.org/10.1007/BF00120423.

Begum, B.A., Hossain, A., Nahar, N., Markwitz, A., Hopke, P.K., 2012. Organic and black carbon in pm2.5 at an urban site at dhaka, Bangladesh. Aerosol and Air Quality Research 12 (6), 1062–1072. https://doi.org/10.4209/aaqr.2012.05.0138.

Bond, T.C., Doherty, S.J., Fahey, D.W., Forster, P.M., Berntsen, T., Deangelo, B.J., Flanner, M.G., Ghan, S., K??rcher, B., Koch, D., Kinne, S., Kondo, Y., Quinn, P.K., Sarofim, M.C., Schultz, M.G., Schulz, M., Venkataraman, C., Zhang, H., Zhang, S., Bellouin, N., Guttikunda, S.K., Hopke, P.K., Jacobson, M.Z., Kaiser, J.W., Klimont, Z., Lohmann, U., Schwarz, J.P., Shindell, D., Storelvmo, T., Warren, S.G., Zender, C.S., 2013. Bounding the role of black carbon in the climate system: a scientific assessment. J. Geophys. Res. Atmos. 118 (11), 5380–5552.

Carbone, S., Saarikoski, S., Frey, A., Reyes, F., Reyes, P., Castillo, M., Gramsch, E., Oyola, P., Jayne, J., Worsnop, D., Hillamo, R., 2013. Chemical characterization of submicron aerosol particles in santiago de Chile. Aerosol Air Qual. Res. 13 (2), 462–473.

Collaud Coen, M., Weingartner, E., Apituley, A., Ceburnis, D., Fierz-Schmidhauser, R., Flentje, H., Henzing, J.S., Jennings, S.G., Moerman, M., Petzold, A., Schmid, O., Baltensperger, U., 2010. Minimizing light absorption measurement artifacts of the aethalometer: evaluation of five correction algorithms. Atmos. Meas. Tech 3 (2), 457–474.

D'Angiola, A., Dawidowski, L.E., Gómez, D.R., Osses, M., 2010. On-road traffic emissions in a megacity. Atmos. Environ. 44 (4), 483–493.

de Miranda, R.M., de Fatima Andrade, M., Fornaro, A., Astolfo, R., de Andre, P.A., Saldiva, P., 2012. Urban air pollution: a representative survey of PM 2.5 mass concentrations in six Brazilian cities. Air Qual. Atmos. Heal 5 (1), 63–77.

Dos Santos, M., Dawidowski, L., Smichowski, P., Ulke, A.G., Gómez, D., 2012. Factors controlling sea salt abundances in the urban atmosphere of a coastal South American megacity. Atmos. Environ. 59, 483–491.

Draxler, R.R., Hess, G., 1998. An overview of the HYSPLIT_4 modelling system for trajectories, dispersion, and deposition. Aust. Meteorol. Mag. 47, 295–308 June 1997.

Drinovec, L., Mocnik, G., Zotter, P., Prévôt2, A.S.H., Ruckstuhl, C., Coz, E., Rupakheti, M., Sciare, J., Müller, T., Wiedensohler, A., Hansen, A.D.A., 2015. The "dual-spot" Aethalometer: an improved measurement of aerosol black carbon with real-time loading compensation. Atmos. Meas. Tech 8 (5), 1965–1979.

El Entre Ríos, E.I., 2015. Quemas programadas en El Palmar. Accessed: 2017-07-27. http://colon.elentrerios.com/sociedad/quemas-programadas-en-el-palmar.htm.

Favez, O., Cachier, H., Sciare, J., Sarda-Estève, R., Martinon, L., 2009. Evidence for a significant contribution of wood burning aerosols to PM2.5 during the winter season in Paris, France. Atmos. Environ. 43 (22–23), 3640–3644.

Favez, O., El Haddad, I., Piot, C., Boréave, A., Abidi, E., Marchand, N., Jaffrezo, J.L., Besombes, J.L., Personnaz, M.B., Sciare, J., Wortham, H., George, C., D'Anna, B., 2010. Inter-comparison of source apportionment models for the estimation of wood burning aerosols during wintertime in an Alpine city (Grenoble, France). Atmos. Chem. Phys. 10 (12), 5295–5314.

Fujiwara, F.G., Gómez, D.R., Dawidowski, L., Perelman, P., Faggi, A., 2011. Metals associated with airborne particulate matter in road dust and tree bark collected in a megacity (Buenos Aires, Argentina). Ecol. Indicat. 11 (2), 240–247.

Fuller, G.W., Tremper, A.H., Baker, T.D., Yttri, K.E., Butterfield, D., 2014. Contribution of wood burning to PM10 in London. Atmos. Environ. 87, 87–94.

Garg, S., Chandra, B.P., Sinha, V., Sarda-Esteve, R., Gros, V., Sinha, B., 2016. Limitation of the use of the absorption angstrom exponent for source apportionment of equivalent black carbon: a case study from the north west indo-gangetic plain. Environ. Sci. Technol. 50 (2), 814–824.

Garreaud, R., Falvey, M., 2008. The coastal winds off western subtropical South America in future climate scenarios. Int. J. Clim 29, 543–554.

Gramsch, E., Reyes, F., Vásquez, Y., Oyola, P., Rubio, M.A., 2016. Prevalence of freshly generated particles during pollution episodes in Santiago de Chile. Aerosol Air Qual. Res. 16 (9), 2172–2185.

Hagler, G.S.W., Yelverton, T.L.B., Vedantham, R., Hansen, A.D.A., Turner, J.R., 2011. Post-processing method to reduce noise while preserving high time resolution in aethalometer real-time black carbon data. Aerosol Air Qual. Res. 11 (5), 539–546.

Herich, H., Hueglin, C., Buchmann, B., 2011. A 2.5 year's source apportionment study of black carbon from wood burning and fossil fuel combustion at urban and rural sites in Switzerland. Atmos. Meas. Tech 4 (7), 1409–1420.

Jeong, C.H., Hopke, P.K., Kim, E., Lee, D.W., 2004. The comparison between thermal-optical transmittance elemental carbon and Aethalometer black carbon measured at multiple monitoring sites. Atmos. Environ. 38 (31), 5193–5204.

Kalnay, E., Kanamitsu, M., Kistler, R., Collins, W., Deaven, D., Gandin, L., Iredell, M., Saha, S., White, G., Woollen, J., Zhu, Y., Chelliah, M., Ebisuzaki, W., Higgins, W., Janowiak, J., Mo, K.C., Ropelewski, C., Wang, J., Leetmaa, A., Reynolds, R., Jenne, R., Joseph, D., 1996. The NCEP/NCAR 40-year Reanalysis Project.

Kistler, R., Kalnay, E., Collins, W., Saha, S., White, G., Woollen, J., Chelliah, M., Ebisuzaki, W., Kanamitsu, M., Kousky, V., Dool, H.V.D., Jenne, R., Fiorino, M., 1999. The NCEP NCAR 50-year Reanalysis : monthly Means CD-ROM and Documentation. pp. 247–268 March 1996.

Laborde, M., Crippa, M., Tritscher, T., Jurányi, Z., Decarlo, P.F., Temime-Roussel, B., Marchand, N., Eckhardt, S., Stohl, A., Baltensperger, U., Prévôt, A.S.H., Weingartner, E., Gysel, M., 2013. Black carbon physical properties and mixing state in the European megacity Paris. Atmos. Chem. Phys. 13 (11), 5831–5856.

Lin, N.-h., Sayer, A.M., Wang, S.-h., Loftus, A.M., Hsiao, T.-c., Sheu, G.-r., Hsu, N.C., Tsay, S.-c., Chantara, S., 2014. Interactions between biomass-burning aerosols and clouds

over Southeast Asia : current status, challenges, and perspectives. Environ. Pollut. 195, 292–307. https://doi.org/10.1016/j.envpol.2014.06.036.
Omar, A.H., Winker, D.M., Kittaka, C., Vaughan, M.A., Liu, Z., Hu, Y., Trepte, C.R., Rogers, R.R., Ferrare, R.A., Lee, K.P., Kuehn, R.E., Hostetler, C.A., 2009. The CALIPSO automated aerosol classification and lidar ratio selection algorithm. J. Atmos. Ocean. Technol. 26 (10), 1994–2014.
Oreggioni, G.F. d. I., 2010. Evolución de las emisiones provenientes de la combustión fósil originadas en fuentes fijas en el Área Metropolitana de Buenos Aires (1970-2006). Ph.D. thesis. Buenos Aires University.
Park, S.S., Hansen, A.D.A., Cho, S.Y., 2010. Measurement of real time black carbon for investigating spot loading effects of Aethalometer data. Atmos. Environ. 44 (11), 1449–1455. https://doi.org/10.1016/j.atmosenv.2010.01.025.
Pereira, G., Freitas, S.R., Caria, E., Jesus, N., Edemir, Y., Brahmananda, V., Longo, K.M., 2009. Estimating trace gas and aerosol emissions over South America : relationship between fire radiative energy released and aerosol optical depth observations. Atmos. Environ. 43 (40), 6388–6397. https://doi.org/10.1016/j.atmosenv.2009.09.013.
Pereira, G., Shimabukuro, Y.E., Moraes, E.C., Freitas, S.R., Cardozo, F.S., Longo, K.M., 2011. Monitoring the transport of biomass burning emission in South America. Atmos. Pollut. Res. 2 (3), 247–254. http://linkinghub.elsevier.com/retrieve/pii/S1309104215304815.
Petzold, A., Ogren, J.A., Fiebig, M., Laj, P., Li, S.M., Baltensperger, U., Holzer-Popp, T., Kinne, S., Pappalardo, G., Sugimoto, N., Wehrli, C., Wiedensohler, A., Zhang, X.Y., Chemistry, A., Atmospheric, P., Techniques, M., 2013. Recommendations for reporting black carbon measurements. Atmos. Chem. Phys. 13 (16), 8365–8379.
Polissar, A., Hopke, P.K., Harris, J., 2001. Source regions for atmospheric measured at Barrow Alaska. Environ. Sci. Technol. 35 (21), 4214–4226.
Reich, S., Magallanes, J., Dawidowski, L., Gómez, D., Grošelj, N., Zupan, J., Aug 2006. An analysis of secondary pollutants in buenos aires city. Environ. Monit. Assess. 119 (1), 441–457. https://doi.org/10.1007/s10661-005-9035-2.
Sandradewi, J., Prévôt, A.S.H., Szidat, S., Perron, N., Alfarra, M.R., Lanz, V.A., Weingartner, E., Baltensperger, U.R.S., 2008a. Using aerosol light absorption measurements for the quantitative determination of wood burning and traffic emission contribution to particulate matter. Environ. Sci. Technol. 42 (9), 3316–3323.
Sandradewi, J., Prévôt, A.S.H., Weingartner, E., Schmidhauser, R., Gysel, M., Baltensperger, U., 2008b. A study of wood burning and traffic aerosols in an Alpine valley using a multi-wavelength Aethalometer. Atmos. Environ. 42 (1), 101–112.
Schmid, O., Artaxo, P., Arnott, W.P., Chand, D., Gatti, L.V., Frank, G.P., Hoffer, a., Schnaiter, M., Andreae, M.O., 2005. Spectral light absorption by ambient aerosols influenced by biomass burning in the Amazon Basin. I: comparison and field calibration of absorption measurement techniques. Atmos. Chem. Phys. Discuss. 5 (5), 9355–9404.
Seguel, A.R., Morales, S.R.G.E., Leiva, G.M.A., 2009. Estimations of primary and secondary organic carbon formation in PM2.5 aerosols of Santiago City, Chile. Atmos. Environ. 43 (13), 2125–2131.
Segura, S., Estellés, V., Titos, G., Lyamani, H., Utrillas, M.P., Zotter, P., Prévôt, A.S.H., Mocnik, G., Alados-Arboledas, L., Martínez-Lozano, J.A., 2014. Determination and analysis of in situ spectral aerosol optical properties by a multi-instrumental approach. Atmos. Meas. Tech 7 (8), 2373–2387.
Snider, G., Weagle, C.L., Martin, R.V., Van Donkelaar, A., Conrad, K., Cunningham, D., Gordon, C., Zwicker, M., Akoshile, C., Artaxo, P., Anh, N.X., Brook, J., Dong, J., Garland, R.M., Greenwald, R., Griffith, D., He, K., Holben, B.N., Kahn, R., Koren, I., Lagrosas, N., Lestari, P., Ma, Z., Vanderlei Martins, J., Quel, E.J., Rudich, Y., Salam, A., Tripathi, S.N., Yu, C., Zhang, Q., Zhang, Y., Brauer, M., Cohen, A., Gibson, M.D., Liu, Y., 2015. SPARTAN: a global network to evaluate and enhance satellite-based estimates of ground-level particulate matter for global health applications. Atmos. Meas. Tech 8 (1), 505–521.
Souto-Oliveira, C.E., Andrade, M. d. F., Kumar, P., Lopes, F. J. d. S., Babinski, M., Landulfo, E., 2016. Effect of local and remote sources and new particle formation events on the activation properties of cloud condensation nuclei in the Brazilian megacity of São Paulo. Atmos. Chem. Phys. Discuss. 1–35. April. http://www.atmos-chem-phys-discuss.net/acp-2016-241/.
Turtos Carbonell, L.M., Sanchez Gacita, M., Rivero Oliva, J.D.J., Curbelo Garea, L., Diaz Rivero, N., Meneses Ruiz, E., 2010. Methodological guide for implementation of the AERMOD system with incomplete local data. Atmos. Pollut. Res. 1 (2), 102–111. http://www.atmospolres.com/articles/Volume1/issue2/APR-10-013.pdf.
Ulke, A.G., Torres Brizuela, M.M., Raga, G.B., Baumgardner, D., 2016. Aerosol properties and meteorological conditions in the city of Buenos Aires, Argentina, during the resuspension of volcanic ash from the Puyehue-Cordón Caulle eruption. Nat. Hazards Earth Syst. Sci. 16 (9), 2159–2175. http://www.nat-hazards-earth-syst-sci.net/16/2159/2016/.
UNEP, 2011. Near-term climate protection and clean air benefits : actions for controlling short-lived climate forcers. Tech. Rep.
Uria-tellaetxe, I., Carslaw, D.C., 2014. Environmental modelling & software conditional bivariate probability function for source identification. Environ. Model. Softw 59, 1–9. https://doi.org/10.1016/j.envsoft.2014.05.002.
Weingartner, E., Saathoff, H., Schnaiter, M., Streit, N., Bitnar, B., Baltensperger, U., 2003. Absorption of light by soot particles: determination of the absorption coefficient by means of aethalometers. J. Aerosol Sci. 34 (10), 1445–1463.
Yerramsetti, V.S., Sharma, A.R., Gauravarapu Navlur, N., Rapolu, V., Dhulipala, N.S.K.C., Sinha, P.R., 2013. The impact assessment of Diwali fireworks emissions on the air quality of a tropical urban site, Hyderabad, India, during three consecutive years. Environ. Monit. Assess. 185 (9), 7309–7325.
Young, S.A., Vaughan, M.A., 2009. The retrieval of profiles of particulate extinction from cloud-aerosol lidar infrared pathfinder satellite observations (CALIPSO) data: algorithm description. J. Atmos. Ocean. Technol. 26 (6), 1105–1119. http://journals.ametsoc.org/doi/abs/10.1175/2008JTECHA1221.1.
Zanatta, M., Gysel, M., Bukowiecki, N., Müller, T., Weingartner, E., Areskoug, H., Fiebig, M., Yttri, K.E., Mihalopoulos, N., Kouvarakis, G., Beddows, D., Harrison, R.M., Cavalli, F., Putaud, J.P., Spindler, G., Wiedensohler, A., Alastuey, A., Pandol, M., Sellegri, K., Swietlicki, E., Jaffrezo, J.L., Baltensperger, U., Laj, P., 2016. A European Aerosol Phenomenology-5 : Climatology of Black Carbon Optical Properties at 9 Regional Background Sites across Europe, vol 145. pp. 346–364.
Zha, S., Cheng, T., Tao, J., Zhang, R., Chen, J., Zhang, Y., Leng, C., Zhang, D., Du, J., 2014. Characteristics and relevant remote sources of black carbon aerosol in Shanghai. Atmos. Res. 135–136, 159–171. https://doi.org/10.1016/j.atmosres.2013.09.002.
Zhu, T., Melamed, M., Parrish, D., Gauss, M., Gallardo Klenner, L., 2013. WMO/IGAC Impacts of megacities on air pollution and climate. Tech. Rep. 205. http://www.wmo.int/pages/prog/arep/gaw/documents/Final{_}GAW{_}205{_}web{_}31{_}January.pdf.